



Enhanced northward propagation of boreal summer intraseasonal oscillation in the western north Pacific linked to the tropical Indian Ocean warming

Young-Min Yang^{1,6,7} · June-Yi Lee^{2,3} · Doo Young Lee⁴ · Bin Wang⁵

Received: 19 September 2023 / Accepted: 30 August 2024
© The Author(s) 2024

Abstract

While decadal changes in Madden–Julian oscillation (MJO) have received considerable attention, the corresponding changes in Boreal Summer Intraseasonal Oscillation (BSISO) have yet to be well understood. In this study, we show the enhanced northward propagation of BSISO in the Western North Pacific (WNP) during the 2000s compared to the 1980s–1990s. Observational analyses and model experiments suggest this enhancement is partially attributed to the tropical Indian Ocean (TIO) warming. The TIO warming tends to increase the air–sea interaction, enhancing moisture anomalies in the free atmosphere. Consequently, this increase in moisture anomalies strengthens BSISO-scale convection through increased convective anomalies at the north of the BSISO center, thereby enhancing the northward propagation of BSISO. Additionally, vorticity changes resulting from mean-state zonal vertical shear also contribute to the BSISO decadal change. Our findings underscore the importance of considering the interaction between BSISO and changes in the ocean mean state in future assessments.

Keywords Boreal summer intraseasonal oscillation · Northward propagation · Tropical Indian ocean warming · NESM3.0 · Air–sea interaction

✉ Young-Min Yang
ymyang@jbnu.ac.kr

✉ June-Yi Lee
juneyi@pusan.ac.kr

¹ Department of Environment & Energy, Jeonbuk National University, Jeonju-si, Republic of Korea

² Research Center for Climate Sciences and Department of Climate System, Pusan National University, Busan, South Korea

³ Center for Climate Physics, Institute for Basic Science (IBS), Busan, South Korea

⁴ Institute of Ocean and Atmospheric Science (IOAS), Hanyang University, Ansan, South Korea

⁵ Department of Atmosphere Science and International Pacific Research Center, University of Hawaii, Honolulu, HI, USA

⁶ School of Civil, Environmental, Resources and Energy Engineering, Jeonbuk National University, Jeonju-si, Republic of Korea

⁷ Soil Environment Research Center, Jeonbuk National University, Jeonju-si, Republic of Korea

1 Introduction

Boreal summer intraseasonal oscillation (BSISO) is characterized by significant northward propagation in the western North Pacific (WNP) and Indian Ocean (e.g., Wang and Rui 1990; Zhu and Wang 1993; Hsu and Weng 2001; Lee et al. 2013). In the WNP, the BSISO convection propagates from the equator to the subtropical western Pacific. It is well known that the BSISO in the WNP is closely associated with the East Asian summer monsoon (e.g., Wang and Xie 1997; Li et al. 2015; Lee et al. 2013, 2017; Hsu et al. 2017), typhoon (Maloney and Hartmann 2001; Goswami et al. 2003; Kikuchi et al. 2009; Moon et al. 2018), and extreme weather and climate events (Moon et al. 2013; Hsu et al. 2016, 2017, 2021).

Several key mechanisms and processes drive the northward propagation of BSISO in the WNP, including vorticity anomalies induced by vertical wind shear, air–sea interaction, and meridional moisture advection. The dynamic theories represented for enhanced vorticity anomalies by wind shear have been suggested in many studies (Wang and Xie 1997; Jiang et al. 2004; Drbohlav and Wang 2005; Yang et al. 2019a, 2020c). Jiang et al. (2004) proposed that

barotropic vorticity anomalies by vertical shear should generate boundary layer moisture convergence (BLMC) to the north of the BSISO convection center, inducing northward propagation of the BSISO. Kemball-Cook and Weare (2001) suggested that warmer sea surface temperature (SST) anomalies by reduced evaporation could contribute to generating the next convection at the north of the BSISO precipitation center, inducing northward propagation of the BSISO convection. The air-sea interaction could lead to warmer SST anomalies and increases convective instability to the north of the BSISO convection center, and thus the convection moves northward (Fu et al. 2003; Fu and Wang 2004; Zheng et al. 2004). Katsumata et al. (2011) suggested warmer SST anomalies induce moistening in the lower troposphere north of the BSISO center, which may be necessary for the northward propagation of the BSISO. Hsu and Weng (2001) found that evaporation may be increased by positive feedback between convection and associated circulation, contributing to abundant moisture around the South China Sea. DeMott et al. (2013) found that the meridional structure of moisture anomalies and the barotropic vorticity effect could contribute to the northward propagation of the BSISO in the WNP. Yang et al. (2020a, b, c) demonstrated that the air-sea interaction plays a critical role in BSISO northward propagation in the WNP, while the barotropic vorticity mechanism is the major driver in the Indian Ocean.

While the decadal changes in the Madden–Julian Oscillation (MJO) and its associated teleconnections have garnered considerable attention, particularly the intensified MJO activity over the WNP during boreal winter in recent decades (Roxy et al. 2019; Hsu et al. 2021), the corresponding shifts in the BSISO, especially within the WNP, have received less scrutiny. Recent studies have suggested that the rising tropical SST influences the decadal variations in the regional Hadley and Walker circulations through enhanced air-sea coupling (Annamalai and Slingo 2001; Neena and Gowami 2010). Kajikawa et al. (2009) noted significant changes in BSISO behavior over the South China Sea after 1994. Yamaura and Kajikawa (2016) highlighted a decadal shift in BSISO patterns in the eastern Indian Ocean around 2000, linked to warmer SST anomalies, using observed data. Sabeerali et al. (2014) investigated from observation the impact of Tropical Indian Ocean (TIO) warming on the BSISO over the Bay of Bengal, revealing heightened BSISO activity during 2001–2010 compared to 1979–1988. Nonetheless, the decadal changes in the BSISO over the WNP due to TIO warming and the underlying mechanisms remain unclear.

This study aims to explore the decadal shifts in BSISO patterns within the WNP and to discern the dominant processes among potential mechanisms using observation and model experiments. These mechanisms include air-sea interaction, vorticity-wind shear interaction, and the meridional

structure of mean moisture advection. We undertake this investigation through an analysis of observational data and model simulations. The explanation for the data and model experiments is outlined in Sect. 2. Section 3 emphasizes the characteristics of the decadal changes in BSISO northward propagation and delves into the underlying mechanisms through the utilization of various diagnostic tools. Finally, Sect. 4 succinctly summarizes our findings and suggests avenues for further research.

2 The model and diagnostic methods

2.1 Model and experiments

For idealized climate model experiments, this study uses the third version of the Nanjing University of Information Science and Technology Earth System Model (NESM3.0) (Cao et al. 2018; Yang et al. 2020a), which consists of the atmosphere, ocean, sea ice, and land models that are fully coupled by an explicit coupler. The resolution of the atmospheric model was T63L47. The ocean model has a grid resolution of 1° , with a meridional resolution refined to $1/3^\circ$ over the equatorial region. The model uses 46 vertical layers, with the upper 15 in the top 100 m. The convective parameterization is based on Tiedtke (1989) and Nordeng (1994) (TDK, hereafter), and the default setting is from the ECHAM6.3 (Peters et al. 2017; Möbis and Stevens 2012). This convective scheme includes three different types of convection—shallow, deep, and midlevel convection—but allows only one type of cloud when convection occurs. The initiation of deep convection depends on the amount of large-scale moisture convergence. The buoyancy of updrafts is affected by organized entrainment and detrainment, and the entrainment rate is calculated from the buoyancy and vertical velocity of the updraft. The closure of the deep convection scheme is calculated by convective available potential energy (CAPE) (Nordeng 1994). To account for the moisture effect of convective development, the entrainment rates in convective clouds have been increased. An increasing entrainment rate can cause a decrease in deep convection due to mixing between the updraft and relatively dry and cold ambient air. In the convective scheme, the cloud top is determined by the entrainment rate, which is estimated by the convective velocity and buoyancy of convective clouds (Möbis and Stevens 2012). We include the effect of the relative humidity of the ambient air. We assume that the entrainment rate (ϵ) is parameterized based on buoyancy and grid-mean humidity, following Kim and Kang (2012). The stratiform cloud scheme implements a cloud microphysical scheme and a diagnostic cloud cover scheme.

The NESM3.0 reproduces reasonable climatology and realistic MJO and BSISO (Yang and Wang 2019; Yang et al.

2019a, b, 2020b). In the model simulations, the northward propagation of BSISO is well reproduced over both the WNP and Indian Ocean. To investigate the impact of TIO warming on the BSISO, we conducted 50-year simulations by nudging the fixed observed SST averaged over 2001–2010 in the tropical Indian Ocean (EXP1) and decreased the tropical Indian Ocean SST uniformly by 1 °C (EXP2) and 2 °C (EXP3). The model was freely coupled in other areas, and external forcings based on the CMIP6 historical simulation protocol were fixed during the integration to remove the increase in SST by anthropogenic forcing over the western Pacific and other regions. The initial conditions were obtained from an ensemble mean of historical runs from CMIP6 protocols.

2.2 The data and diagnostic methods

Daily mean outgoing longwave radiation (OLR) data are obtained from the National Oceanic and Atmospheric Administration (NOAA) (Liebmann and Smith 1996). The Global Precipitation Climatology Project (GPCP) daily data (Adler et al. 2003) are used for precipitation, and the European Center for Medium-Range Weather Forecast Reanalysis 5 (ERA) daily data (Hersbach et al. 2020) are utilized for circulation during 1979–2020. We use a 20–70-day band-pass filter to obtain the ISO signal during the boreal summer season (May 1st to October 31st). Based on dynamics-based diagnostics, we analyzed the relationship between circulation, SST, moisture, and BSISO northward propagation. Tropical Indian Ocean index is defined by SST averaged over 10°S–10°N and 40°E–100°E from May to October. We define the BSISO index as the first two leading modes of Multi-Variate-EOF analysis of daily mean Outgoing Longwave Radiation (OLR) and 850-hPa zonal wind (U850) anomalies over the Asian Summer Monsoon (ASM) region (10°S–40°N, 40°–160°E) from May 1st to October 31st for the 40 years from 1981 to 2020 based on Lee et al. (2013). The OLR and U850 anomalies were obtained by removing the slow annual cycle (mean and first three harmonics of climatological annual variation) as well as the effect of interannual variability by subtracting the running mean of the last 120 days. We did not apply any other time filtering.

3 Effects of the tropical Indian Ocean warming on mean fields and BSISO

We examined the decadal changes using the BSISO and TIO indices. Figure 1 illustrates the annual BSISO activity (Fig. 1a) and the TIO index (Fig. 1c), both averaged from May to October. The BSISO index was calculated following the method of Lee et al. (2013) and the BSISO activities were calculated by the square root of the sum of the squares

of the first two principal components. The dashed line represents the decadal component of each time series. Notably, the decadal BSISO index shows relatively minor and negative values for 1979–1999, while it exhibits significant positive values for 2000–2011. The differences in BSISO activity between periods P1 and P2 were statistically significant at approximately the 1% level (as shown in Table 1), underscoring substantial decadal shifts around the year 2000. Additionally, we calculated the BSISO index using the methods developed by Kikuchi et al. (2012). The results also indicate significant decadal changes in the BSISO index (Fig. 1b), suggesting that these decadal changes in the BSISO index are robust. Prior research has identified decadal alterations in the BSISO over the Indian Ocean during the 2000s. Consequently, we have defined two distinct periods, namely period 1 (P1, 1986–1995) and period 2 (P2, 2001–2010), to effectively assess the impacts of TIO warming on the BSISO. Note that the decadal variability of the BSISO index defined by the Real-time Multivariate MJO index (Wheeler and Hendon 2004) exhibits relatively weak decadal change compared to other methods, which may be due to meridional asymmetry in the decadal change of the BSISO (not shown).

3.1 Changes in the boreal summer mean climate

Figure 2 depicts the disparities in mean-state SST, zonal wind, and moisture at 850 hPa between periods P2 and P1 (P2 minus P1) in observation and model simulations. The SST contrast reveals substantial warming across the western equatorial Pacific, alongside comparatively milder warming in the subtropical western Pacific (Fig. 2a). The meridional SST gradient exhibits a discernible increase extending from the equatorial western Pacific to 15°N. These SST alterations could impact the average moisture levels and air-sea interactions that influence the northward propagation of BSISO. The mean-state moisture of P2 in the free atmosphere is more abundant than that in P1. Contrasting with the easterly winds during period P1, the low-level easterly winds in P2 notably diminish from the equator to 25°N over the western Pacific, resulting in prominent positive values (Fig. 2b). These reductions in zonal wind may potentially affect the augmented zonal vertical shear and the accompanying vorticity anomalies.

The model reasonably reproduces the observed meridional SST structure and zonal wind patterns. In EXP2, the meridional gradient of mean-state SST is slightly smaller than that in EXP1 (Fig. 2a, blue line). Importantly, it's worth noting that the warming of the western Pacific in the model simulation could potentially be attributed to TIO warming, considering that anthropogenic forcings remain unchanged in the model simulations. The mean-state moisture tends to increase with TIO warming (Fig. 2c), which is consistent

Fig. 1 a, b Time series of the normalized BSISO index (solid blue line) (10°S–10°N, 40°–100°E) averaged from May to October, with the decadal component of the normalized BSISO index (dashed blue line) based on Lee et al. (a, 2013) and Kikuchi et al. (b, 2012). Decadal components is defined by 5-year running average. The left x-axis indicates the strength of BSISO activity (no unit). c same as a but for Tropical Indian ocean (TIO) SST. The left x-axis denotes TIO index (°C)

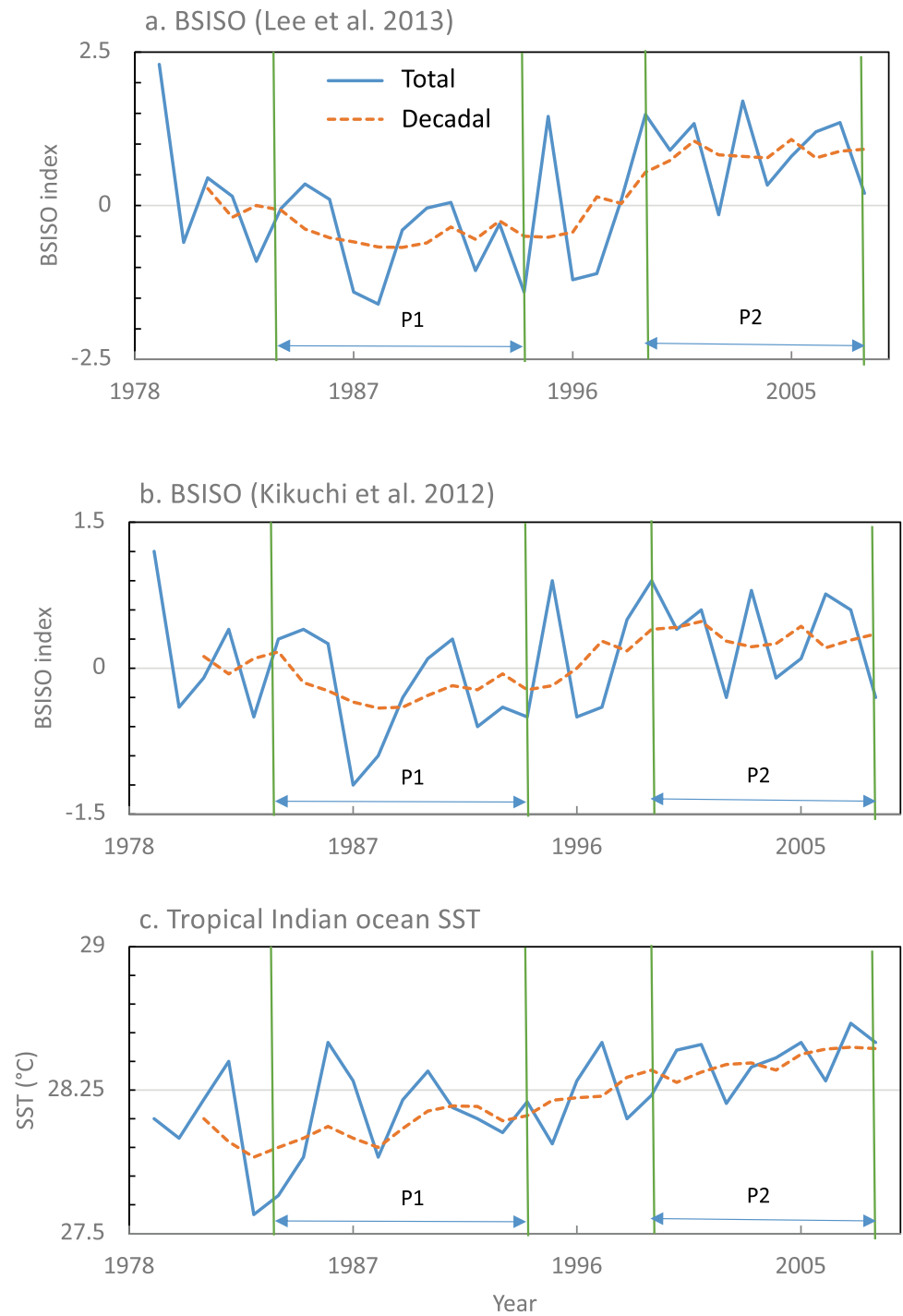


Table 1 Probability of the monthly averaged BSISO index following a student t-test during P1 and P2

Index	May	Jun	Jul	Aug	Sep	Oct
P2-P1	0.02	0.68	0.08	0.02	0.05	0.06

with the observation. Furthermore, the easterly zonal wind in EXP2 intensifies over the subtropical western Pacific compared to EXP1. Notably, the disparities between EXP1

and EXP2 align well with the corresponding observations (Fig. 2b, blue line). The inclusion of additional cooling in EXP3 accentuates the differences in SST and zonal wind

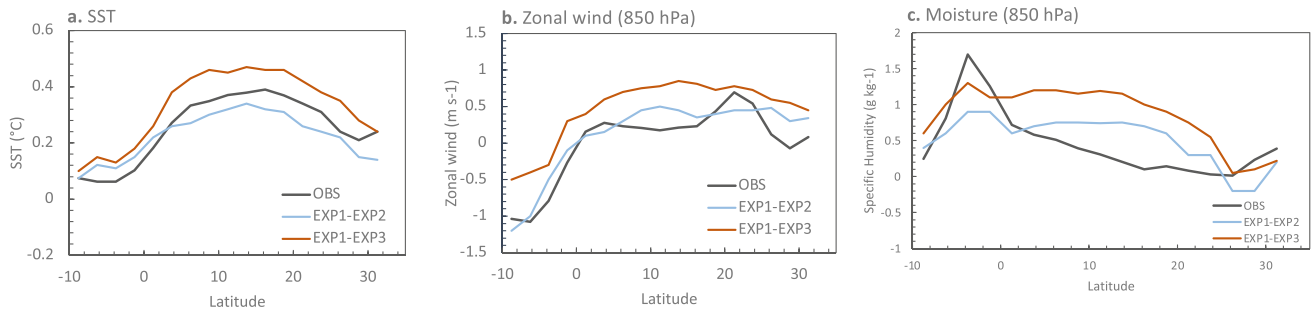


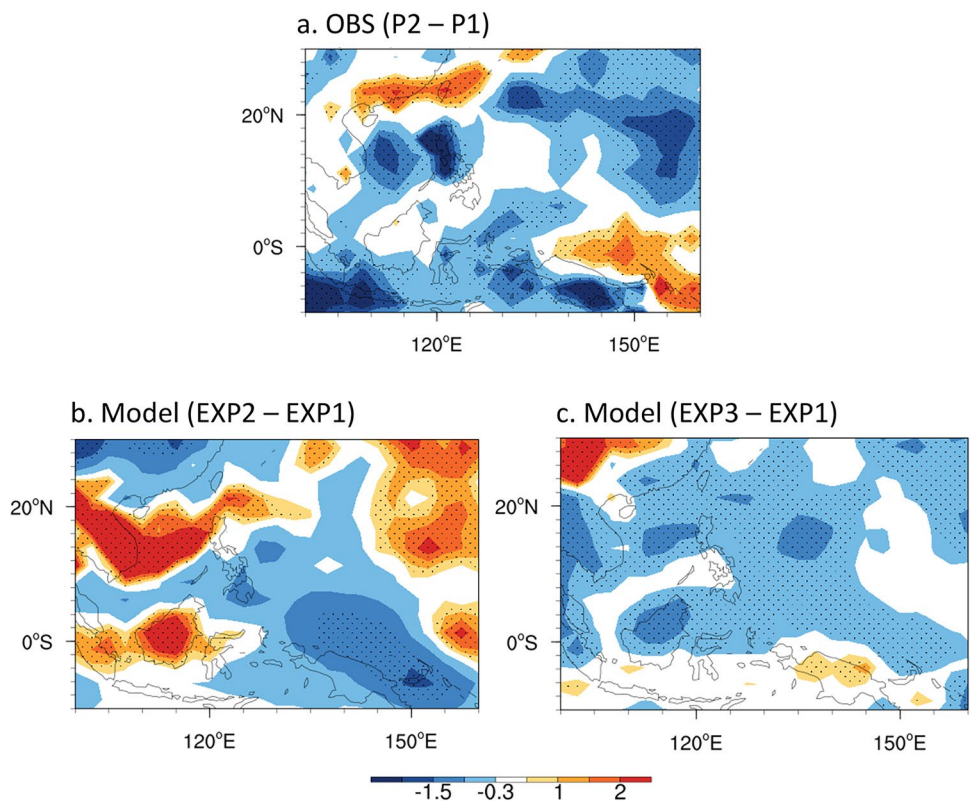
Fig. 2 Difference of Meridional structure of May–November **a** mean-state SST (°C), **b** zonal wind ($m s^{-1}$) and **c** specific humidity ($g kg^{-1}$) at 850 hPa averaged over 125°–145°E from observation between P2 and P1 (black lines) and model simulations (color lines)

between EXP1 and EXP3 (Fig. 2, red line), surpassing those between EXP1 and EXP2. Consequently, the results from the model experiments indicate that TIO warming could indeed contribute to the observed decadal changes in the mean-state climate.

Figure 3a shows the June–August mean state differences in precipitation between P2 and P1. The difference between the P2 and P1 experiments indicates a decrease in precipitation over the eastern part of the Maritime Continent and the western Pacific, particularly the South China Sea and the Philippines. Model simulations show reduced

mean precipitation due to TIO warming. The difference between EXP2 and EXP1 (Fig. 3b) shows a decrease in precipitation due to TIO warming over the eastern part of the Maritime Continent and the western Pacific. From the difference between EXP1 and EXP3, reduced precipitation was seen over the western Pacific, the South China Sea, and the Maritime Continent (Fig. 3c). These results suggest that TIO warming reduces mean precipitation in the western Pacific and the Maritime Continent. The reduced mean precipitation in the Maritime Continent may contribute to the weakened northward propagation of the BSISO.

Fig. 3 Difference in June–August mean state precipitation ($mm day^{-1}$) from observations and model experiments. Dotted area represents significance at 95% level



3.2 Changes in BSISO properties

Composite life cycles of outgoing longwave radiation (OLR) and horizontal wind vectors at 850 hPa associated with the BSISO are analyzed to examine the changes in the propagation structures of BSISO in the western Pacific. Utilizing daily anomalies of OLR and zonal wind at 850 hPa (U850) within the range of 10°S–10°N, 40°–160°E, we employed a multivariate empirical orthogonal function (EOF) analysis as recommended by Lee et al. (2013). Defining eight phases using the first and second EOF modes, as these modes capture the canonical northward propagating mode, we examine the period spanning from May to October.

Figure 4 illustrates phases 4 to 6 of the BSISO during this period. In P2, robust convective anomalies related to BSISO are observed in the Maritime continent and the equatorial western Pacific during phase 4 (upper panel of Fig. 4b). Observation shows a northwest-southeast tilted structure extending from the western Indian Ocean to the western North Pacific. These anomalies propagate both eastward and northward, intensifying and peaking in the

Western North Pacific at phase 5 (middle panel of Fig. 4b). Notably, these convective anomalies propagate northward from the southern Philippine Sea to the South China Sea, with their magnitude slightly diminishing by Phase 6 (lower panel of Fig. 4b). In contrast, during P1, distinct alterations are observed in convective anomalies and associated circulation. In phase 4, the peak of convective anomalies emerges in the eastern Indian Ocean rather than the Maritime continent (upper panel of Fig. 4a). These convective anomalies move eastward and northward. However, their intensity in the western Pacific does not amplify during phase 5, rendering them weaker than those in P2 (middle panel of Fig. 4a). Moreover, the convective anomalies do not progress northward, and their signals largely dissipate.

Model simulations reveal a reinforced northward propagation of the BSISO due to TIO warming. EXP1 captures a northwest-southeast tilted structure extending from the western Indian Ocean to the western North Pacific in Phase 4, which closely aligns with observations. Additionally, model simulations demonstrate a significant northward movement of BSISO convection from Phase 4 to Phase 6 (Fig. 4c).

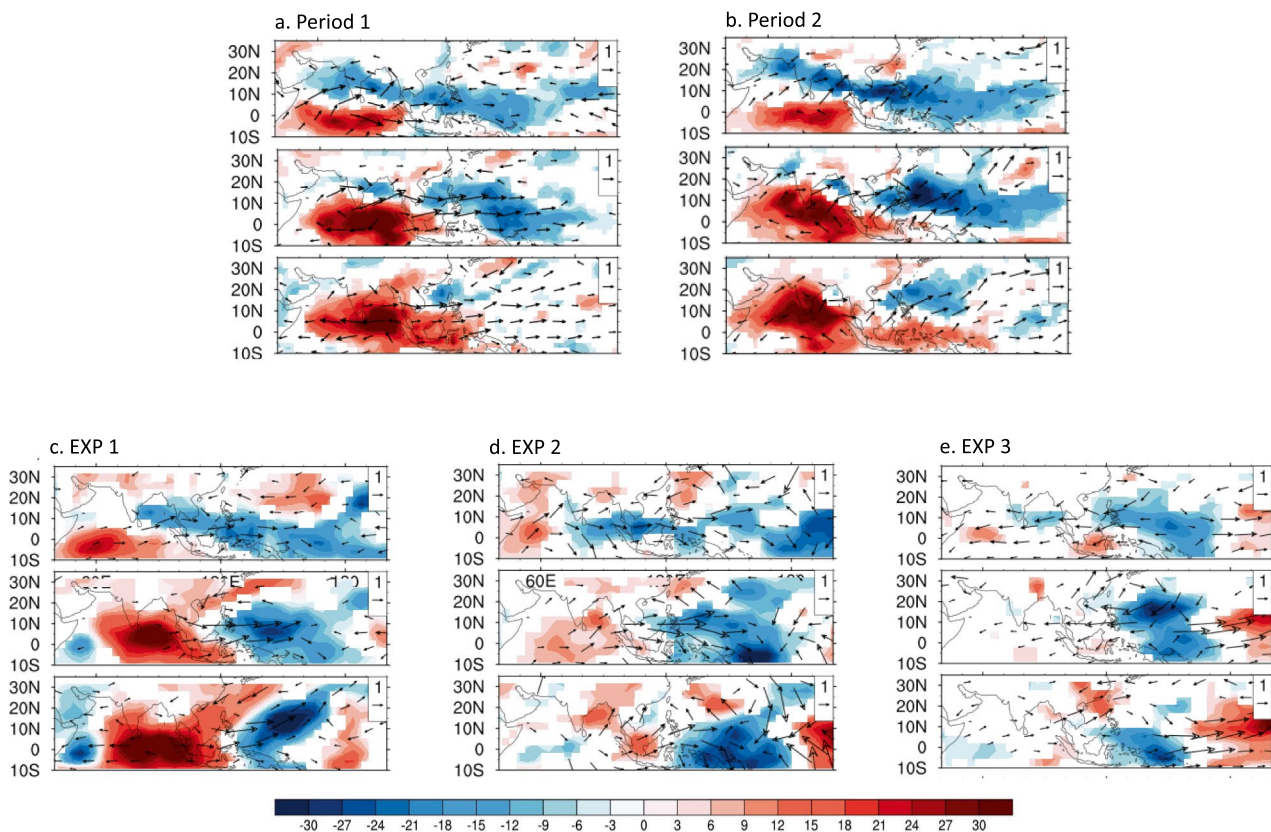


Fig. 4 **a, b** The life cycle composite of OLR (shading, W m^{-2}) and 850-hPa wind (vector, m s^{-1}) anomaly reconstructed based on PC1 and PC2 of BSISO1 in Phases 4 (upper), 5 (middle), and 6 (bottom) during **a** period 1 and **b** period 2 from observation. **c–e** same as **a–b**

but for **c** EXP 1, **d** EXP2, and **e** EXP3. The composite life cycles have a moderate amplitude (1.0). We defined eight phases of ISO based on Lee et al. (2013), the wind vectors are represented with statistical significance at a 95% confidence level based on a t test

Conversely, in EXP2, BSISO convection moves both northward and southward during phase 5 and appears to stall near the equator in phase 6 (Fig. 4d). In EXP3, BSISO convection exhibits slight southward propagation from phase 4 to phase 6 (Fig. 4e). These findings underscore the distinct enhancement of northward propagation in P2 compared to P1, with TIO warming likely playing a contributory role in these observed decadal BSISO changes. Note that intraseasonal signals of EXP2 and EXP3 in the eastern Indian Ocean were substantially reduced, which may be associated with a systematic cold bias of the model in the eastern Indian Ocean. Another possible reason is that in our atmosphere model, the large-scale circulation (e.g., Walker circulation) is highly sensitive to the zonal gradient SST change between the eastern Indian Ocean and the western Pacific. If the Indian Ocean is lowered by 1 degree, the rising motion in the western Indian Ocean could induce anomalous sinking motion in the eastern Indian Ocean, which could contribute to the weakening of the convective anomalies.

Changes in mean-state climate fields between periods P1 and P2 can potentially impact the northward propagation of the BSISO in the western Pacific. To investigate the influence of the Tropical Indian Ocean (TIO) on the latitude-time

structure of the BSISO, we examined the lead-lag correlation of BSISO precipitation in the western Pacific, using the ISO convection center located at the equatorial western Pacific (125°–145°E, 5°S–5°N) as a reference due to its robust BSISO northward propagation. Convection advances northward with a phase speed of 1.25 m s^{-1} from the equatorial western Pacific to the South China Sea (Fig. 5b). In P2, BSISO convection advances northward with a phase speed of 1.3 m/s from the equatorial western Pacific to the South China Sea (Fig. 5b). The correlation coefficient remains consistently between 0.4 and 0.5 up to 25°N. In contrast, during P1, the convection also progresses northward, reaching approximately 15°N, but the correlation coefficient significantly drops by 0.1 beyond 15°N (Fig. 5a). This suggests that the signal for northward propagation is most prominent around the equator and then quickly diminishes in the subtropical western Pacific. Model simulations closely mirror these changes in the northward propagation of the BSISO. In EXP1, BSISO between 0.4 and 0.5 up to 20°N, highlighting the predominance of northward propagation in the subtropical western Pacific (Fig. 5c). Conversely, in EXP2 (weak TIO cooling), the signal for northward propagation weakens from 10° to 25°N compared to EXP1 (Fig. 5d). In EXP3

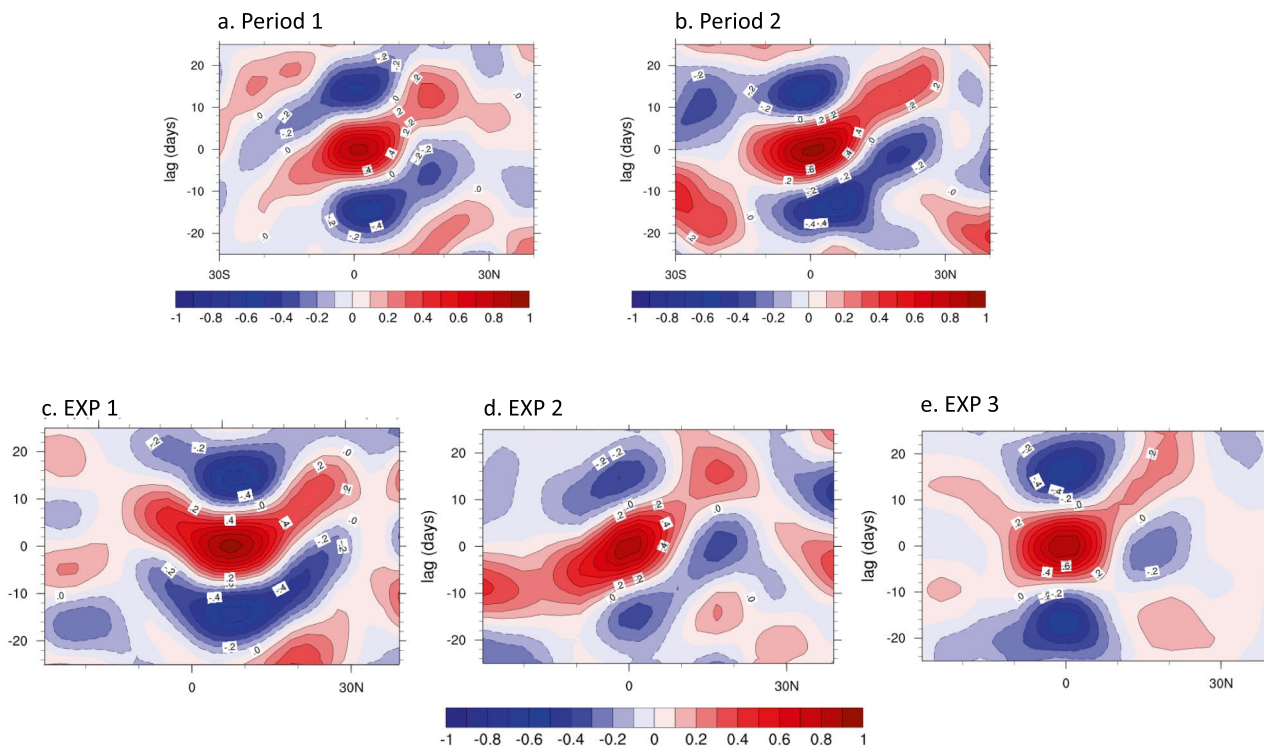


Fig. 5 a, b Propagation of ISO OLR as depicted by the lead-lag correlation of 20–70 day filtered OLR averaged over 125–145°E during a period 1 and b period 2 from observation based on Lee et al. (2013). c–e same as a–b but for c EXP1, d EXP2 and e EXP3. Boreal

summer (May–October) data are used for the analysis. The ISO OLR averaged over 125°E–145°E and 5°S–5°N was used as a reference for calculating the correlation

(strong TIO cooling), the signal for the northward propagation of the BSISO is greatly weakened, with a small correlation coefficient of 0.1–0.2 (Fig. 5e). The model results collectively suggest that alterations in mean-state conditions prompted by Tropical Indian Ocean (TIO) warming play a partial role in enhancing the northward propagation of the BSISO in the western North Pacific.

4 Potential underlying mechanisms

Based on observational analysis and model simulations, we propose potential mechanisms for the weakening of BSISO northward propagation in the WNP driven by TIO warming. The warming of the TIO results in increased SST over the equatorial western Pacific, which triggers enhanced deep convection. This, in turn, intensifies the Hadley circulation and induces alterations in temperature and wind patterns in both the lower and upper troposphere, notably enhancing zonal vertical wind shear (Fig. 6a). During period P2, substantial easterly vertical wind shear is evident from the equatorial western Pacific to the subtropical western Pacific (10°S–20°N), with its peak at 10°N before diminishing. In contrast, during period P1, vertical wind shear weakens in the southern equatorial to subtropical western Pacific (10°S–30°N) in comparison to P2. In addition, the lower tropospheric easterlies decrease in P2 compared to P1, leading to a more pronounced zonal vertical wind shear. It's important to note that the differences in upper-tropospheric easterlies between P2 and P1 are much smaller than the differences in low-level zonal winds. In the model simulation, zonal vertical shear tends to be reduced with TIO cooling, which is consistent with the observation. EXP1 shows significant easterly vertical wind shear from the equatorial western Pacific to the subtropical western Pacific (10°S–20°N), but its magnitude is slightly larger than the observation (P2). In EXP2, the easterly vertical shear is reduced as in P1. EXP3

shows very weakened easterly vertical shear, suggesting that TIO warming may contribute to increased easterly vertical shear in the western Pacific.

The changes in zonal vertical wind shear could potentially be attributed to shifts in barotropic vorticity, potentially giving rise to coupled baroclinic and barotropic modes. Regression analysis was conducted to explore the relationship between BSISO convection and vorticity anomalies. Figure 6b illustrates the meridional structure of regressed vorticity anomalies at 925 hPa onto OLR averaged over the western Pacific (5°S–5°N, 125°–145°E). In P2 (solid black line), positive vorticity anomalies are evident from 5°N to 20°N, peaking around 8°N. Conversely, during P1, the peak of vorticity anomalies diminishes and shifts equatorward, with the positive vorticity range contracting from 5°N to 14°N. These reduced positive vorticity anomalies in P1 are consistent with the attenuated zonal vertical wind shear, supporting the link between vorticity anomalies and changes in BSISO convection. In the model simulation, EXP1 shows positive anomalies between 0°N and 20°N with slightly stronger magnitudes. In EXP2 the positive anomalies are reduced compared to those in EXP1. In EXP3, positive anomalies occur only between 0°N and 10°N, suggesting that TIO warming may contribute to enhanced vorticity anomalies.

The positive vorticity anomalies associated with BSISO convection may contribute to enhancing the Boundary Layer Moisture Convergence (BLMC). BLMC can play a role in moistening the lower-level atmosphere and triggering deep convection (e.g., Bladé and Hartmann 1993; Johnson et al. 1999; Kemball-Cook and Weare 2001; Tian et al. 2006). Figure 6c depicts regressed BLMC anomalies at 925 hPa onto OLR averaged over the western Pacific (5°S–5°N, 120°–150°E). In P2, positive BLMC anomalies are observed from 3°S to 18°N, consistent with the meridional pattern of vorticity anomalies (Fig. 6c). The BLMC is nearly absent around the equatorial western Pacific, with its peak

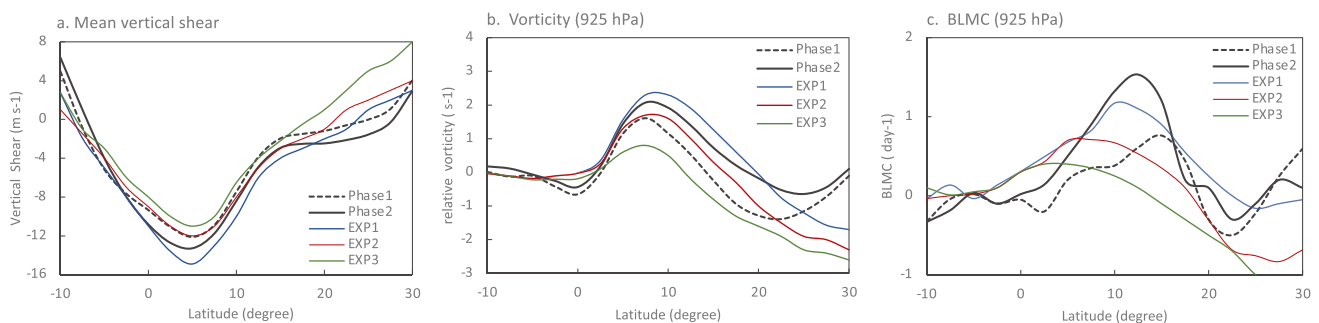


Fig. 6 Meridional structure of May–November **a** mean-state zonal shear (U200 minus U850) averaged over 125°–145°E from observation (black lines) and models (color lines). Meridional variation of the regressed ISO **b** relative vorticity (s^{-1}) at 925 hPa, **c** BL moisture

convergence (day^{-1}) anomalies at 925 hPa averaged over 125°–145°E from observation and model simulations. For **a–b**, The 20–70 day filtered OLR anomaly averaged over 5°S–5°N and 125–145°E was used as a reference for calculating regression

occurring around 13°N, suggesting that subsequent convection might develop to the north of the BSISO center. In comparison, during P1, the positive BLMC extends from 8°N to 18°N, with a relatively smaller peak. The reduced range of positive vorticity and BLMC anomalies in P1 also appears to align with the weakened northward propagation over the subtropical western Pacific, as shown in Fig. 5a and b.

In the model simulation, when the TIO is cooled, the BLMCs are reduced, which aligns with the observations. However, the diminished vorticity anomalies caused by zonal vertical shear cannot fully account for the weakened northward propagation of the BSISO, as these changes in vorticity anomalies are limited to the range of 5°N to 15°N, whereas the alteration in northward propagation of the BSISO spans from 5°N to 25°N. In other words, other mechanisms also may contribute to the weakened northward propagation. In summary, the change in vorticity anomalies due to zonal vertical shear contributes to the weakened northward propagation.

Next, we explore how the air-sea interaction mechanism affects the northward propagation of the BSISO. Figure 7a displays the meridional structure of regressed SST anomalies onto the BSISO convection center. In P2, positive SST anomalies are evident from 5°N to 25°N, aligning with the signal of BSISO northward propagation. In contrast, in P1, positive SST anomalies occur only between 15°N and 22°N, with significantly reduced magnitudes. This reduction may contribute to the weakened northward propagation of ISO convection. Model simulations also show that the SST anomalies in EXP1 are larger than those in EXP2 and EXP3, implying that the next convection in EXP1 (TIO warming) is more likely to occur north of the ISO center compared to EXP2 and EXP3 (TIO cooling). The easterly surface anomalies of P2 decrease from the equator to the subtropical western Pacific compared to those in P1 (Fig. 7c). This reduces the latent heat flux, leading to warming and abundant moisture anomalies. Model simulations support these observations. The easterly surface wind anomalies are reduced with TIO warming. These results suggest that TIO warming may contribute to strengthening the meridional gradient of SST anomalies associated with BSISO convection over the subtropical western Pacific, thereby enhancing the northward

motion of ISO convection. These observations suggest that air-sea interaction may play an important role in explaining the weakened northward propagation caused by TIO warming.

In addition, we investigated the processes related to the role of moisture in the free atmosphere on the northward propagation of BSISO (Jiang et al. 2018; Wang and Sobel 2022). The positive moisture anomalies in the free troposphere could potentially contribute to the generation of the subsequent convection north of the BSISO convection center. Figure 8 illustrates the meridional pattern of moisture anomalies in the free atmosphere. In P2, positive moisture anomalies are evident from 10°S to 15°N, consistent with the signal from the northward propagation of the BSISO. In contrast, in P1, positive moisture anomalies occur only between 0°N and 8°N, with significantly reduced magnitudes. This reduction may inhibit convection north of the BSISO center, contributing to the weakened northward propagation of the ISO convection. Model simulations show that EXP1 captures the observed positive moisture anomalies between 10°S and 15°N. The moisture anomalies in EXP1 are larger than those in EXP2 and EXP3, suggesting

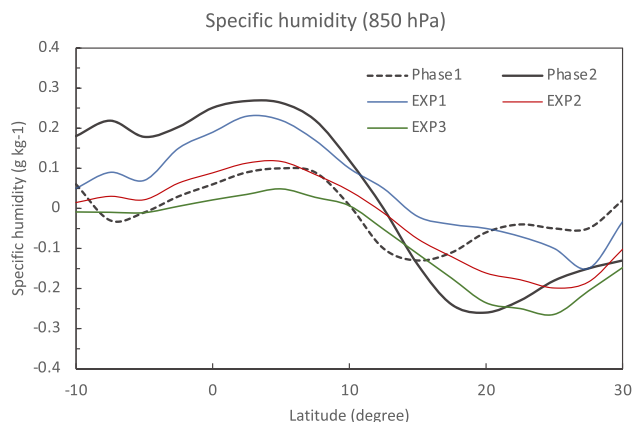
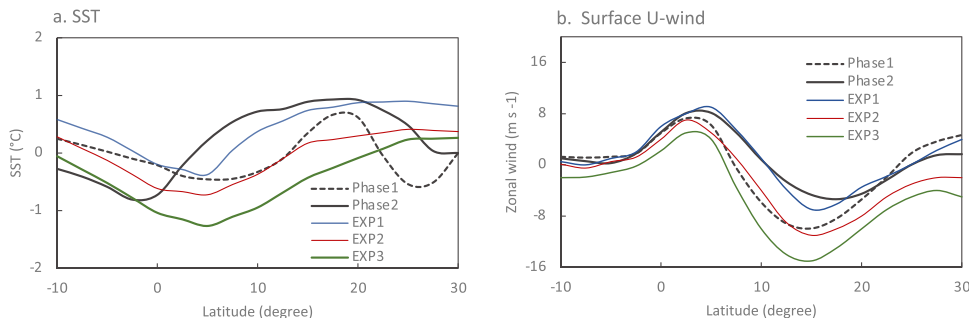


Fig. 8 Meridional variation of the regressed ISO specific humidity anomalies (g kg^{-1}) at 850 hPa averaged over 125°–145°E from observation and model simulations. The 20–70 day filtered OLR anomaly averaged over 5°S–5°N and 125–145°E was used as a reference for calculating regression

Fig. 7 Meridional variation of the regressed ISO **a** SST (K) and **b** surface zonal wind (m s^{-1}) anomalies averaged over 125°–145°E from observation and model simulations. The 20–70 day filtered OLR anomaly averaged over 5°S–5°N and 125–145°E was used as a reference for calculating regression



that the next convection in EXP1 is more likely to occur north of the ISO center compared to EXP2 and EXP. These results imply that TIO warming contributes to better BSISO northward propagation by increasing the moisture in the free atmosphere.

5 Conclusion and discussion

We investigated the influence of the Tropical Indian Ocean (TIO) on the northward propagation of the Boreal Summer Intraseasonal Oscillation (BSISO) in the Western North Pacific (WNP) and examined how TIO warming affects the BSISO signal through a combination of observations and model simulations. We explored several potential mechanisms, including vorticity anomalies induced by vertical zonal wind shear, air-sea interaction processes, and the meridional structure of mean moisture in the boundary layer.

Our findings suggest that TIO warming enhances BSISO northward propagation by amplifying both the air-sea interaction effect and the vorticity effect from zonal vertical shear over the WNP. TIO warming leads to an increased meridional structure of warm sea surface temperature (SST) and moisture anomalies linked to the BSISO convection center, fostering subsequent convection and consequently strengthening the northward propagation of the BSISO. The vorticity anomalies resulting from heightened zonal vertical shear also contribute to the intensified northward propagation.

The amplitude of observed northward propagation during a specific period may also be influenced by interactions with other ocean basins, such as the Atlantic multi-decadal variability or the Pacific decadal oscillation. Recent studies suggest that North Atlantic warming since the 2000s can induce a negative phase of the Pacific decadal oscillation, characterized by warming in the western Pacific and cooling in the eastern Pacific, resulting in a similar meridional structure of mean SST (Hong et al. 2022; Yang et al. 2020a). Another study indicates a linkage between TIO warming and North Atlantic warming, with the latter contributing to TIO warming and influencing the horizontal pattern of the interdecadal Pacific oscillation (Mohtadi et al. 2014; Xie et al. 2021; Yang et al. 2022). The impact of the North Atlantic Ocean (or the negative interdecadal Pacific oscillation) on the BSISO will be investigated in future studies.

To mitigate potential model-dependent outcomes, future research could replicate similar experiments using different climate models to ensure the consistency of results. It's important to acknowledge that the numerical experiments conducted in this study were based on a single model.

Acknowledgements We appreciate the valuable comments and suggestions from anonymous reviewers, which significantly improved the manuscript.

Funding National Research Foundation of Korea, NRF-2022R1A2C1013296 and NRF-2022M3K3A109782, June-Yi Lee, National Science Foundation (NSF) of USA, NSF-2025057, Bin Wang.

Data availability Observed data used for this study are available publicly. The observational atmospheric data sets are available online (NCEP-DOE Reanalysis 2: <https://psl.noaa.gov/data/gridded/data.ncep.reanalysis2.html>, NCEP/NCAR Reanalysis 1: <https://psl.noaa.gov/data/gridded/data.ncep.reanalysis.html>, NOAA's OLR: <https://psl.noaa.gov/data/gridded/data.olrcdr.interp.html>). GPCP precipitation can be obtained from <https://psl.noaa.gov/data/gridded/data.gpcp.html>. NOAA OISST data are provided at <https://psl.noaa.gov/data/gridded/data.noaa.oisst.v2.html>.

Code availability The model data and source code for analysis can be downloaded here: https://figshare.com/articles/dataset/BSISO_TIO_impact/23304818. Software used is bash script, CDO, NCL, and Python.

Declarations

Conflict of interest The authors declare that they have no conflict of interest.

Open Access This article is licensed under a Creative Commons Attribution-NonCommercial-NoDerivatives 4.0 International License, which permits any non-commercial use, sharing, distribution and reproduction in any medium or format, as long as you give appropriate credit to the original author(s) and the source, provide a link to the Creative Commons licence, and indicate if you modified the licensed material. You do not have permission under this licence to share adapted material derived from this article or parts of it. The images or other third party material in this article are included in the article's Creative Commons licence, unless indicated otherwise in a credit line to the material. If material is not included in the article's Creative Commons licence and your intended use is not permitted by statutory regulation or exceeds the permitted use, you will need to obtain permission directly from the copyright holder. To view a copy of this licence, visit <http://creativecommons.org/licenses/by-nc-nd/4.0/>.

References

- Adler RF et al (2003) The version-2 global precipitation climatology project (GPCP) monthly precipitation analysis (1979–present). *J Hydrometeorol* 4(6):1147–1167
- Bladé I, Hartmann DL (1993) Tropical intraseasonal oscillations in a simple nonlinear model. *J Atmos Sci* 50(17):2922–2939
- Cao J, Wang B, Yang Y-M, Ma L, Li J, Sun B, Bao Y, He J, Zhou X, Wu L (2018) The NUIST Earth System Model (NESM) version 3: description and preliminary evaluation. *Geosci Model Dev* 11:2975–2993. <https://doi.org/10.5194/gmd-11-2975-2018>
- DeMott CA, Stan C, Randall DA (2013) Northward propagation mechanisms of the boreal summer intraseasonal oscillation in the ERA-Interim and SP-CCSM. *J Clim* 26:1973–1992
- Drbohlav H-KL, Wang B (2005) Mechanism of the northward propagating intraseasonal oscillation: insights from a zonally symmetric model. *J Clim* 18:952–972
- Fu X, Wang B (2004) Differences of boreal summer intraseasonal oscillations simulated in an atmosphere-ocean coupled model and an atmosphere-only model. *J Clim* 17:1263–1271
- Fu X, Wang B, Li T, McCreary JP (2003) Coupling between northward-propagating, intraseasonal oscillations and sea surface temperature in the Indian Ocean. *J Atmos Sci* 60:1733–1753

- Goswami BN, Ajayamohan RS, Xavier PK, Sengupta D (2003) Clustering of synoptic activity by Indian summer monsoon intraseasonal oscillations. *Geophys Res Lett* 30:1431–1434
- Hong J, Yeh S, Yang Y (2022) Interbasin interactions between the Pacific and Atlantic Oceans depending on the phase of Pacific decadal oscillation and Atlantic multidecadal oscillation. *J Clim* 35:2883–2894
- Hsu H-H, Weng C-H (2001) Northwestward propagation of the intraseasonal oscillation in the Western North Pacific during the boreal summer: structure and mechanism. *J Clim* 14:3834–3850
- Hsu P-C, Lee J-Y, Ha K-J (2016) Influence of boreal summer intraseasonal oscillation on rainfall extremes in southern China. *Int J Climatol* 36:1403–1412
- Hsu P-C, Lee J-Y, Ha K-J, Tsou C-H (2017) Boreal summer intraseasonal oscillation on heat waves in monsoon Asia. *J Clim* 30:7191–7211
- Hsu P-C, Fu Z, Murakami H, Lee J-Y, Yoo C, Johnson NC, Chang C-H, Liu Y (2021) East Antarctic cooling induced by decadal changes in Madden-Julian oscillation during austral summer. *Sci Adv* 7:eabf9903
- Jiang X, Li T, Wang B (2004) Structures and mechanisms of the northward propagating boreal summer intraseasonal oscillation. *J Clim* 17:1022–1039
- Jiang X, Adames ÁF, Zhao M, Waliser D, Maloney E (2018) A unified moisture mode framework for seasonality of the Madden-Julian oscillation. *J Clim* 31:4215–4224
- Johnson RH et al (1999) Trimodal characteristics of tropical convection. *J Clim* 12(8):2397–2418
- Katsumata M, Ciesielski PE, Johnson RH (2011) Evaluation of budget analysis during MISMO. *J Appl Meteorol Climatol* 50:241–254
- Kikuchi K, Wang B, Fudeyasu H (2009) Genesis of tropical cyclone Nargis revealed by multiple satellite observations. *Geophys Res Lett* 36:L06811. <https://doi.org/10.1029/2009GL037296>
- Kikuchi K, Wang B, Kajikawa Y (2012) Bimodal representation of the tropical intraseasonal oscillation. *Clim Dyn* 38(9–10):1989–2000. <https://doi.org/10.1007/s00382-011-1159-1>
- Kim D, Kang IS (2012) A bulk mass flux convection scheme for climate model: description and moisture sensitivity. *Clim Dyn* 38:411–429
- Lee J-Y, Wang B, Wheeler MC, Fu X, Waliser DE, Kang I-S (2013) Real-time multivariate indices for the boreal summer intraseasonal oscillation over the Asian summer monsoon region. *Clim Dyn* 40:493–509
- Lee J-Y, Kwon M, Yun K-S, Min S-K et al (2017) The long-term variability of Changma in the East Asian summer monsoon system: a review and revisit. *Asia-Pac J Atmos Sci* 53:257–272
- Li K, Li Z, Yang Y, Xiang B, Liu Y, Yu W (2015) Strong modulations on the Bay of Bengal monsoon onset vortex by the first northward-propagating intra-seasonal oscillation. *Clim Dyn* 47:107–115
- Liebmann B, Smith CA (1996) Description of a complete (interpolated) outgoing longwave radiation dataset. *Bull Am Meteor Soc* 77:1275–1277
- Maloney ED, Hartmann DL (2001) The Madden-Julian oscillation, Barotropic dynamics, and North Pacific tropical cyclone formation: part I—observations. *J Atmos Sci* 58:2545–2558
- Möbis B, Stevens B (2012) Factors controlling the position of the inter-tropical convergence zone on an aquaplanet. *J Adv Model Earth Syst* 4(4):M00A04
- Mohtadi M et al (2014) North Atlantic forcing of tropical Indian Ocean climate. *Nature* 509:76–80
- Moon J-Y, Wang B, Ha K-J, Lee J-Y (2013) Teleconnections associated with Northern Hemisphere summer monsoon intraseasonal oscillation. *Clim Dyn* 40:2761–2774. <https://doi.org/10.1007/s00382-012-1394-0>
- Moon JY, Wang B, Lee S-S, Ha K-J (2018) An intraseasonal genesis potential index for tropical cyclones during northern hemisphere summer. *J Clim* 31(22):9055–9071
- Nordeng TE (1994) Extended versions of the convective parametrization scheme at ECMWF and their impact on the mean and transient activity of the model in the tropics. European Centre for Medium-Range Weather Forecasts
- Roxy MK, Dasgupta P, McPhaden MJ et al (2019) Twofold expansion of the Indo-Pacific warm pool warps the MJO life cycle. *Nature* 575:647–651
- Tian B et al (2006) Vertical moist thermodynamic structure and spatial-temporal evolution of the MJO in AIRS observations. *J Atmos Sci* 63(10):2462–2485
- Wang B, Rui H (1990) Dynamics of the coupled moist Kelvin-Rossby wave on an equatorial β -plane. *J Atmos Sci* 47(4):397–413
- Wang S, Sobel AH (2022) A unified moisture mode theory for the Madden-Julian oscillation and the Boreal summer intraseasonal oscillation. *J Clim* 35(4):1267–1291
- Wang B, Xie X (1997) A model for the boreal summer intraseasonal oscillation. *J Atmos Sci* 54:72–86
- Wheeler MC, Hendon HH (2004) An all-season real-time multivariate MJO index: development of an index for monitoring and prediction. *Mon Weather Rev* 132:1917–1932
- Xie T et al (2021) Origin of Indian Ocean multidecadal climate variability: role of the North Atlantic oscillation. *Clim Dyn* 56:3277–3294
- Yang Y-M, Wang B (2019) Improving MJO simulation by enhancing the interaction between boundary layer convergence and lower tropospheric heating. *Clim Dyn* 52:4671–4693
- Yang Y-M, Wang B, Lee J-Y (2019a) Mechanisms of northward propagation of boreal summer intraseasonal oscillation revealed by climate model experiments. *Geophys Res Lett* 46:3417–3425
- Yang Y-M, Lee J-Y, Wang B (2019b) The Tibetan Plateau uplift is crucial for eastward propagation of Madden-Julian oscillation. *Sci Rep* 9:15478
- Yang Y-M, An S-I, Wang B, Park JH (2020a) A global-scale multidecadal variability driven by Atlantic multidecadal oscillation. *Nat Sci Rev*. <https://doi.org/10.1093/nsr/nwz216>
- Yang Y-M, Wang B, Cao J et al (2020b) Improved historical simulation by enhancing moist physical parameterizations in the climate system model NESM3.0. *Clim Dyn* 54:3819–3840
- Yang Y-M, Lee J-Y, Wang B (2020c) Dominant process for northward propagation of Boreal summer intraseasonal oscillation over the Western North Pacific. *Geophys Res Lett* 47:e2020GL089808
- Yang YM, Park JH, An SI et al (2022) Increased Indian Ocean-North Atlantic Ocean warming chain under greenhouse warming. *Nat Commun* 13:3978
- Zheng Y, Waliser DE, Stern W, Jones C (2004) The role of coupled sea surface temperatures in the simulation of the tropical intraseasonal oscillation. *J Clim* 17:4109–4134
- Zhu B, Wang B (1993) The 30–60-day convection seesaw between the tropical Indian and western Pacific Oceans. *J Atmos Sci* 50:184–199